tvst

https://doi.org/10.1167/tvst.8.3.57

Article

A New Approach for the Segmentation of Three Distinct Retinal Capillary Plexuses Using Optical Coherence Tomography Angiography

Qiujian Zhu[1,2], Xiaoying Xing[3], Manhui Zhu[2], Haixiang Xiao[2], Lie Ma[2], Lili Chen[2], Juan Liang[2], You Yuan[2], and E. Song[2]

[1] Department of Ophthalmology, The Second Affiliated Hospital of Soochow University, Suzhou, China
[2] Department of Ophthalmology, Lixiang Eye Hospital of Soochow University, Suzhou, China
[3] Suzhou Eye Hospital, Suzhou, China

Correspondence: E. Song, Department of Ophthalmology, Lixiang Eye Hospital of Soochow University, Ganjiang East Road No. 200, Suzhou 215021, China. e-mail: songe@suda.edu.cn

Received: 19 February 2019
Accepted: 3 May 2019
Published: 28 June 2019

Keywords: optical coherence tomography angiography; OCT; OCTA; segmentation; retina; macular capillary plexus

Citation: Zhu Q, Xing X, Zhu M, Xiao H, Ma L, Chen L, Liang J, Yuan Y, Song E. A new approach for the segmentation of three distinct retinal capillary plexuses using optical coherence tomography angiography. Trans Vis Sci Tech. 2019;8(3):57, https://doi.org/10.1167/tvst.8.3.57

Purpose: To segment three distinct retinal capillary plexuses by using optical coherence tomography angiography (OCTA).

Methods: This prospective study included 30 eyes of 15 healthy subjects. En face OCTA images generated by the AngioPlex platform were manually segmented by the "progressive matching" method to the superficial, middle, and deep capillary plexuses (SCP, MCP, and DCP, respectively). The estimated position of each plexus relative to the reference line was calculated. Vascular density (VD) and skeleton density (SD) analyses, as well as the interclass correlation coefficient and relative standard deviation, were performed on each capillary plexus. We also measured central retinal thickness (CRT) and ganglion cell layer thickness (GCT).

Results: Thirty eyes of 15 healthy subjects (9 females; average age of 28.33 $\pm$ 3.07 years) were included in the analysis. We defined the relative estimated positions of the outer boundary MCP to the RPEfit as MCP = 14.491 − 0.307 CRT − 1.443 GCT, while the outer boundary of DCP was 37.63 $\pm$ 7.04 μm below the IPL. The VDs of SCP, MCP, and DCP were 32.97% $\pm$ 3.90%, 45.05% $\pm$ 5.34%, and 37.34% $\pm$ 4.96%, respectively, while the SDs of SCP, MCP, and DCP were 14.45 $\pm$ 1.51 mm^{-1}, 19.80 $\pm$ 1.92 mm^{-1}, and 17.38 $\pm$ 1.97 mm^{-1}, respectively.

Conclusions: With the progressive matching method, we segmented three capillary plexuses and defined the relative estimated positions of each capillary plexus to the reference line and calculated the VD and SD of three capillary plexuses in healthy subjects, providing controls for future studies.

Translational Relevance: Our study provides a visual method for OCTA image vascular segmentation and provides reference and control for future studies on retinal three capillary plexuses.

Introduction

Optical coherence tomography angiography (OCTA) is an advanced, noninvasive, dye-less imaging technology that allows for direct evaluation of the retinal microvasculature with depth-resolved capability.[1–4] The technique is based on the principle of identifying the temporal evolution of the optical coherence tomography (OCT) signal caused by the motion of scattering particles, such as erythrocytes, within the vessels. This technique can be used to generate information on three-dimensional blood flow for visualization of the retinal and choroidal vasculature.[5]

OCTA studies have largely concentrated on the superficial capillary plexus (SCP) and deep capillary plexus (DCP).[2,5–7] However, significant evidence from histopathological and anatomical studies indicates the existence of a third capillary plexus, the middle capillary plexus (MCP), which is controlled by

distinct developmental cues.[8–11] Moreover, according to other studies in rodent and human retina, each capillary layer of the retina has different regulatory units, suggesting an independent neurovascular unit at each capillary plexus, favorably supporting the existence of the MCP.[12–14] Given that the MCP is partially incorporated into other plexuses by standard commercial software, some pioneers began to identify the MCP by manual segmentation of OCTA volumes and came to realize the importance of MCP.[15–17] Nesper et al.[18] even described the three-dimensional image of the three capillary plexuses in their study. However, the position of the MCP is a matter of opinion. Onishi et al.[15] and Park et al.[16] considered the MCP a thin slab between the inner plexiform layer (IPL) and inner nuclear layer (INL) (0 μm offset from IPL and 30 μm beneath the IPL). Hagag and colleagues[14] argued that the MCP is in the outer 20% of the ganglion cell complex and inner 50% of the INL. The approach of Garrity et al.[17] is to segment the MCP with an inner boundary set at the IPL-INL junction and an outer boundary set at 20 μm below the IPL-INL junction. By contrast, Nesper et al.[18] considered that the MCP was segmented from 55 to 6 μm above the IPL. In addition, most previous studies on MCP were performed using the RTVue XR Avanti OCTA instrument (Optovue, Fremont, CA) based on split-spectrum amplitude-decorrelation angiography software, and there are few studies performed using other devices.

In this study, we used the Cirrus high-definition OCT AngioPlex instrument (Zeiss Meditec, Inc., Dublin, CA) by using the Optical Micro Angiography (OMAG) algorithm to segment the three distinct retinal capillary plexuses. A manual segmentation method called "progressive matching" was adopted to determine the locations of MCP and DCP and then calculated their approximate distribution in healthy human subjects by recording their specific locations. In addition, vascular density (VD) and skeleton density (SD) analyses were performed on each capillary plexus. Our study is an important extension of previous studies on three distinct retinal capillary plexuses and provides a basis for future research.

Methods

This prospective study was approved by the Lixiang Eye Hospital of Soochow University Institutional Review Board and adhered to the tenets of the Declaration of Helsinki and was Health Insurance Portability and Accountability Act compliant. Informed consent was obtained from each subject before OCTA imaging.

Study Sample

A total of 15 volunteers were recruited for this study, and a total of 30 normal eyes were evaluated. Each subject underwent a standard refractive diopter (D) measurement (AR-310A; Nidek, Aichi, Japan), slit-lamp biomicroscopy, and dilated fundus examination. The inclusion criteria were no evidence of ocular media opacity, retinal disease, or significant refractive error (myopia of three Ds or more or hyperopia of one D or more) in the study eye. Exclusion criteria included ocular surgery, poor-quality images with a signal strength less than 9 (maximum of 10), significant motion artifact, or inability to abstain from blinking or movement during image acquisition. No eyes were excluded in this study.

OCTA Imaging

Images were obtained using the commercially available instrument Zeiss Cirrus HD-OCT 5000-2328 (Zeiss Meditec, Inc.) with OMAG AngioPlex (software version 9.5.2.19038, copyright 2016). Because the OMAG algorithm does not split the OCT spectrum into subbands, it theoretically provides a higher axial resolution of approximately 5 μm in tissue.[18] The device, with a central wavelength of 840 nm and a scan speed of 68,000 A-scans per second, minimized the effect of eye motion-related artifacts by the use of Fast Trace, as previously described.[5,19] At least one 3×3-mm (759×759 pixels) scan centered on the fovea was taken in each eye of interest.

Segmentation of the Capillary Plexuses

The data were segmented using commercially available AngioPlex software inner-limiting membrane (ILM) and retinal pigment epithelium (RPE-fit) segmentation algorithms, and the position of the IPL was calculated by the two algorithms.[5] According to the user manual of the device, ZIPL = ZILM + 70% * (TILM-OPL), while ZOPL = ZRPEfit − 110 μm; ZIPL is the estimated IPL boundary, ZILM is the ILM boundary, TILM-OPL is the thickness between the ILM and outer plexiform layer (OPL), and ZOPL is the estimated OPL boundary. Because the ILM line encroached upon choroidal vessels in the fovea area when moving down because of the concave area in the fovea, RPEfit and IPL were selected for manual segmentation simultaneously. A

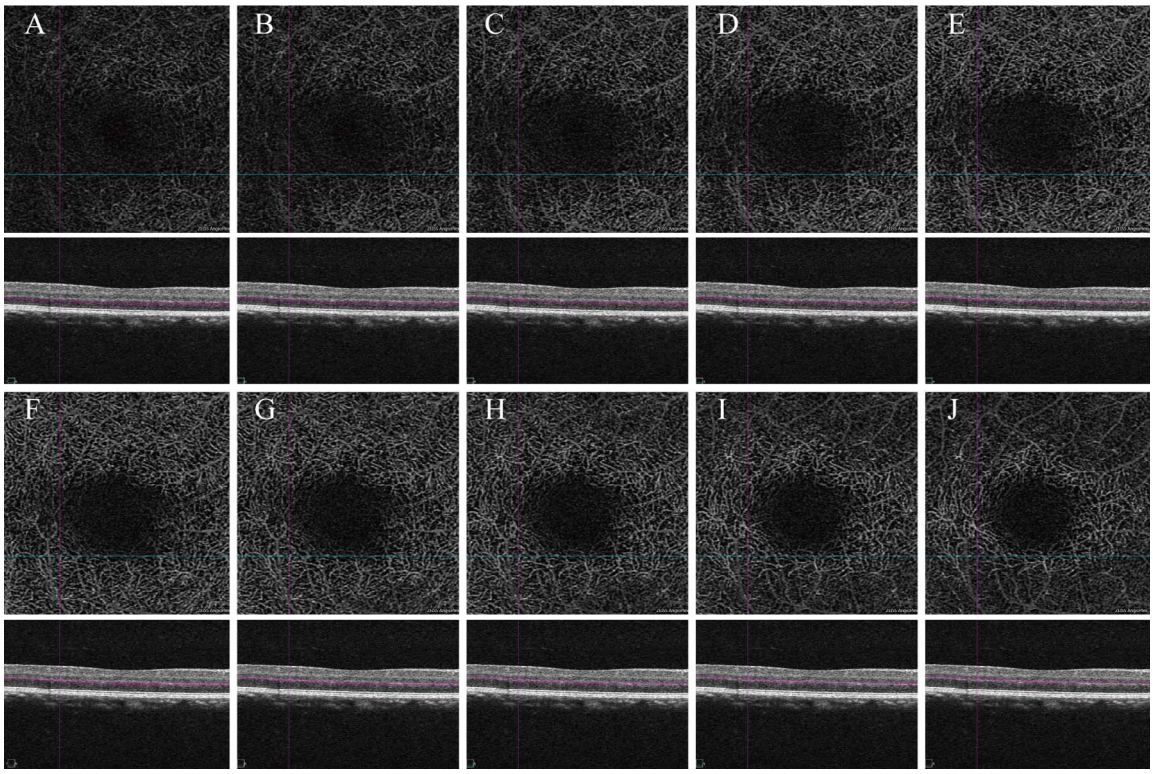

Figure 1. Segmentation of DCPs on OCTA. Right eye of subject (subject identifier [ID] LX201802011). (A–J) A 20-μm-thin slab gradually moved inward from the nonvascular area of the outer nuclear layer at an interval of 6 μm until the continuous capillary plexuses began to disconnect to capture the DCP. G contained the most complete vascular structure and was considered the DCP. The *red lines* on cross-sectional OCTA show the segmentation boundaries for each layer.

manual segmentation method called progressive matching was adopted to determine the locations of MCP and DCP. First, a 20-μm thin slab was set with RPEfit as the reference line and gradually moved upward from the nonvascular area of the outer nuclear layer at an interval of 6 μm until the continuous vascular layer began to disconnect (as shown in Fig. 1). The most integrated image was selected as the DCP, and the relative estimated position from RPEfit was recorded (the outer boundary, same as follows). Then, we adjusted the thin slab to 30 μm and continued to obtain the MCP (as shown in Fig. 2). We repeated the above steps with the IPL as the reference line. The selection of the most integrated image was interpreted by the two independent researchers together, and if the two researchers' interpretation results were inconsistent, the final interpretation was conducted by the third researcher. We further activated the manual "Remove Projections" option in AngioPlex software for MCP and DCP analyses, which uses additive mixing of overlying vessels to reduce projection artifacts in lower layers.[20] In this way, we obtained the MCP and DCP after removal of the decorrelation tail artifact (MCP-re and DCP-re).

Image Analysis

En face OCTA images were exported to an external software program (ImageJ, version 1.50i; http://imagej.nih.gov/ij/; provided in the public domain by the National Institutes of Health, Bethesda, MD, USA) and opened in image analysis.[21] To calculate the VD and SD, we applied a thresholding algorithm to en face images of each capillary plexus to create a binarized black-and-white slab. VD was calculated as a proportion of the total area of pixels with a detected OCTA signal (white pixels in the binarized image) compared to the total area of pixels in the binarized image. From this slab, a skeletonized slab was created, representing vessels with a trace of 1 pixel in width. SD was defined as the ratio of the skeletal length of vessels to the total area of the image (Fig. 4). A similar approach has been described in detail in many previous reports.[1–3,5]

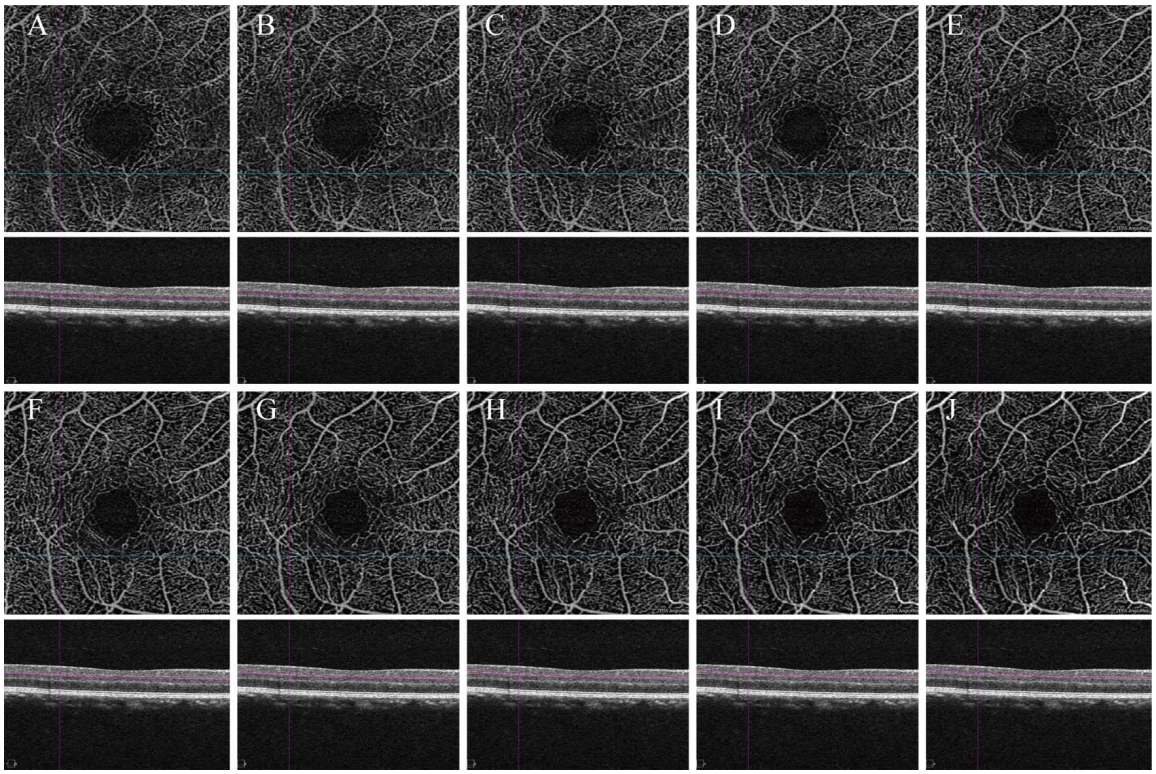

Figure 2. Segmentation of MCPs on OCTA. Right eye of subject (subject ID LX201802011). (A–J) A 30-μm-thin slab continued to move upward at an interval of 6 μm until the vascular structure details began to disappear to capture the MCP. G contained the most complete vascular structure details and was considered MCP. The *red lines* on cross-sectional OCTA show the segmentation boundaries for each layer.

A Cirrus OCT scan of the macula consisting of 128 B-scans with 512 A-scans each (Macular Cube 512 × 128 scan) was taken of each eye, and the central retinal thickness (CRT) and ganglion cell inner plexiform thickness (GCT) were measured using the existing algorithm available on the Cirrus device.

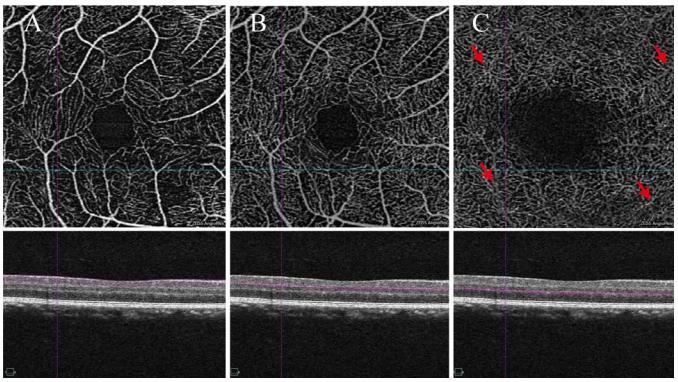

Figure 3. Segmentation of three capillary plexuses on OCTA. En face (*top row*) and cross-sectional (*bottom row*) OCTA of the SCP (A), MCP (B), and DCP (C). The red lines on cross-sectional OCTA show the segmentation boundaries for each layer. The *red arrows* indicate the "vortex" system.

One week later, we randomly selected 20 eyes for resegmentation and analysis to calculate the interclass correlation coefficient (ICC). Moreover, one eye was selected randomly from the segmentation procedure for analysis repeated 10 times to calculate the relative standard deviation (RSD).

Statistical Analysis

Statistical analysis was performed using SPSS 18.0 (IBM Corp., Armonk, NY). For all tests, P values <0.05 were considered statistically significant. All data are reported as the means and standard deviations (SD). Pearson and Spearman correlations were used to study the association between the estimated location of each capillary plexus and the CRT and GCT. A linear regression model (method = stepwise, criteria = pin (0.05) pout (0.10)) was used to calculate the estimated location of the MCP and DCP outer boundaries.

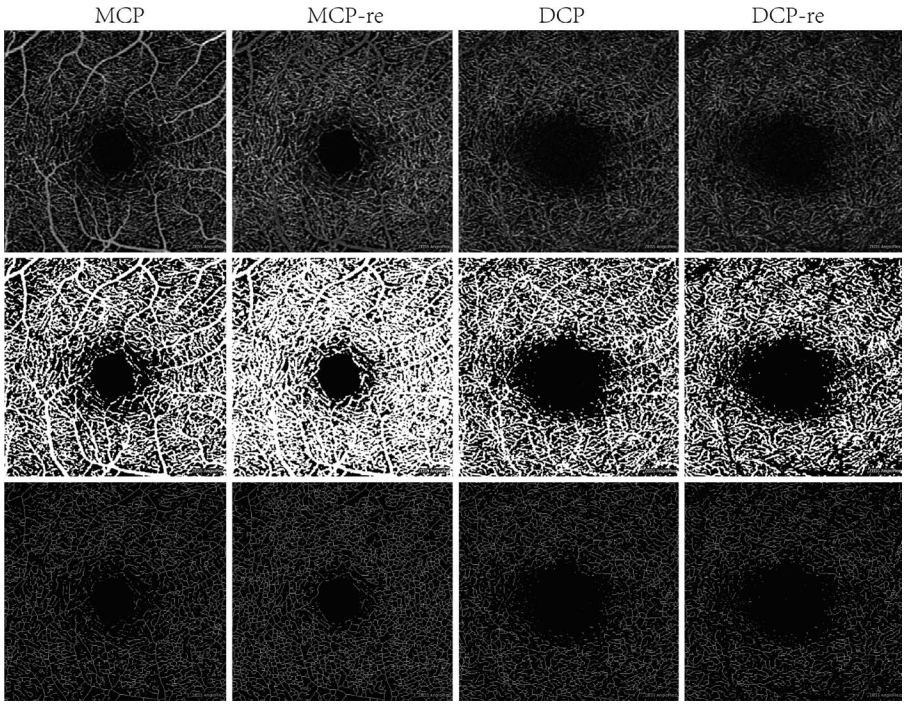

Figure 4. Analysis of the MCP and DCP. *Top row* is the 8-bit image converted from the original image. *Middle row* is the binary image used to calculate the VD, and bottom row is the skeleton image used to calculate the SD. MCP-re means the MCP after removal of the decorrelation tail artifact, and DCP-re means the DCP after removal of the decorrelation tail artifact.

Results

Of the 15 subjects, 9 (60%) were female with an overall average age of 28.33 ± 3.07 (range, 24 to 34) years, and average spherical equivalent of −0.54 ± 0.77 (range, +0.5 to −2.5) D. All images met the entry criteria. Out of a total of 60 interpretations, 7 (11.67%) required a third-party determination (6 for MCP and 1 for DCP).

The outer boundaries of the MCP were 183.30 ± 13.22 μm from the RPEfit and 15.70 ± 8.03 μm from the IPL, while the outer boundaries of the DCP were 137.60 ± 11.42 μm above the RPEfit and 37.63 ± 7.04 μm beneath the IPL (Table 1). The inner boundaries of the MCP were approximately located at the junction of the IPL with the ganglion cell layer (Fig. 2), while the GCT was approximately 85.97 ± 3.32 μm. Because the three networks around the foveal avascular zone (FAZ) would be anastomosed postnatally, we defined the SCP as a slab from 0 μm beneath the ILM to 70 μm beneath the ILM.[9,22] This definition preserves the integrity of the vessels surrounding the FAZ without encroaching upon the MCP in the parafoveal region.

In the Pearson and Spearman correlation analysis, the estimated position of the MCP was strongly correlated with the CRT and GCT relative to RPEfit and IPL, while the estimated position of the DCP was weakly correlated only with the CRT and GCT relative to RPEfit (Table 2).

Linear regression indicated that the estimated position of the MCP relative to RPEfit was correlated with the CRT and GCT, while the estimated position relative to the IPL was affected by the CRT. The position of DCP relative to RPEfit was related to the GCT, while the estimated position relative to IPL was unaffected by either area (Table 3). The estimated

Table 1. Relative Estimated Position of Each Capillary Plexus With Each Reference Line and CRT and GCT[a]

MCP		DCP			
RPEfit (μm)	IPL (μm)	RPEfit (μm)	IPL (μm)	CRT (μm)	GCT (μm)
−183.30 ± 13.22	−15.70 ± 8.03	−137.60 ± 11.42	37.63 ± 7.04	240.33 ± 21.26	85.97 ± 3.32

[a] Data are mean ± standard deviation, and the minus sign means above the reference line.

Table 2. Pearson and Spearman Correlations between the Relative Estimated Position, CRT, and GCT

	MCP				DCP			
	RPEfit (μm)		IPL (μm)		RPEfit (μm)		IPL (μm)	
	Pearson	Spearman	Pearson	Spearman	Pearson	Spearman	Pearson	Spearman
CRT								
R	−0.650	−0.640	−0.478	−0.475	−0.408	−0.449	−0.210	−0.346
P	<0.001[a]	<0.001[a]	0.008[a]	0.008[a]	0.025[b]	0.012[b]	0.266	0.061
GCT								
R	−0.575	−0.547	−0.476	−0.460	−0.455	−0.415	−0.321	−0.335
P	0.001[a]	0.002[a]	0.008[a]	0.011[b]	0.012[b]	0.023[b]	0.084	0.070

[a] Means $P < 0.01$.
[b] Means $P < 0.05$.

position of MCP relative to RPEfit had a high degree of fitting with the CRT and GCT (adjusted $R^2 = 0.494$) and had a better prediction accuracy (Fig. 5). Therefore, the outer boundary of MCP relative to the estimated position of RPEfit was set as Y, CRT as X_1, and GCT as X_2, and the regression equation $Y = 14.491 - 0.307X_1 - 1.443X_2$ was given.

The SCP was mainly composed of arteries, veins, arterioles, and venules arranged around the center, whereas the MCP and DCP were mainly composed of arterioles, venules, and a large number of capillaries (Figs. 3, 4). In the DCP, we also found some "vortex" systems (red arrow), which drain into central conduits that directly connect to venules in the SCP, as previously described.[18,23,24] Among the three retinal capillary plexuses, the MCP had the highest VD (45.05% ± 5.34%), followed by the DCP (37.34% ± 4.96%), and the lowest was SCP (32.97% ± 3.90%). After the artifact was removed, the VD of the DCP-re decreased (33.42% ± 4.80%), but the VD of the MCP-re increased (57.52% ± 7.11%). Similar results were found for SD, as shown in Table 4.

Table 3. Linear Regression Analysis With the Relative Estimated Position, CRT, and GCT[a]

	Unstandardized Coefficient	Standardized Coefficient	*P* Value
MCP-RPEfit	Adjusted $R^2 = 0.494$, Constant = 14.491		
CRT	−0.307	−0.493	0.002
GCT	−1.443	−0.362	0.020
MCP-IPL	Adjusted $R^2 = 0.201$, Constant = 27.696		
CRT	−0.181	−0.478	0.008
GCT	-	-	-
DCP-RPEfit	Adjusted $R^2 = 0.178$, Constant = −2.950		
CRT	-	-	-
GCT	−1.566	−0.455	0.012
DCP-IPL	Adjusted $R^2 = 0.043$		
CRT	-	-	-
GCT	-	-	-

[a] Method = stepwise, criteria = pin (0.05) pout (0.10).

VD showed high reproducibility with ICCs more than 0.941 for each capillary plexus, and SD showed high reproducibility with ICCs more than 0.931 for each capillary plexus. Both VD and SD showed high precision, with RSDs less than 2.26% for each capillary plexus. Table 5 showed the detailed results of the ICCs and RSDs.

Discussion

In this study, we used a progressive matching method for segmentation, which has good reproducibility and precision according to the ICC and RSD tests. To ensure the accuracy of the results, we used two judges to interpret together and introduced a third judge when the interpretation was inconsistent. The interpretation of the DCP was more consistent, whereas the MCP was more prone to divergence in interpretation due to the influence of SCP decorrelation tail artifacts.

For the thickness of the DCP, Onishi et al.[15] and Park et al.[16] selected a thin slab of 15 μm, but we found that a slab of this thickness could not display an integrated DCP; thus, we selected a thin slab of 20 μm to segment the DCP following the method of Bonnin et al.[25]

DCP is presumably located on the lateral side of the INL and most of the OPL, whereas the MCP is presumably located at the inner edge of the INL and most of the IPL. There was a distinct disruption of the vascular layer inside the INL. According to develop-

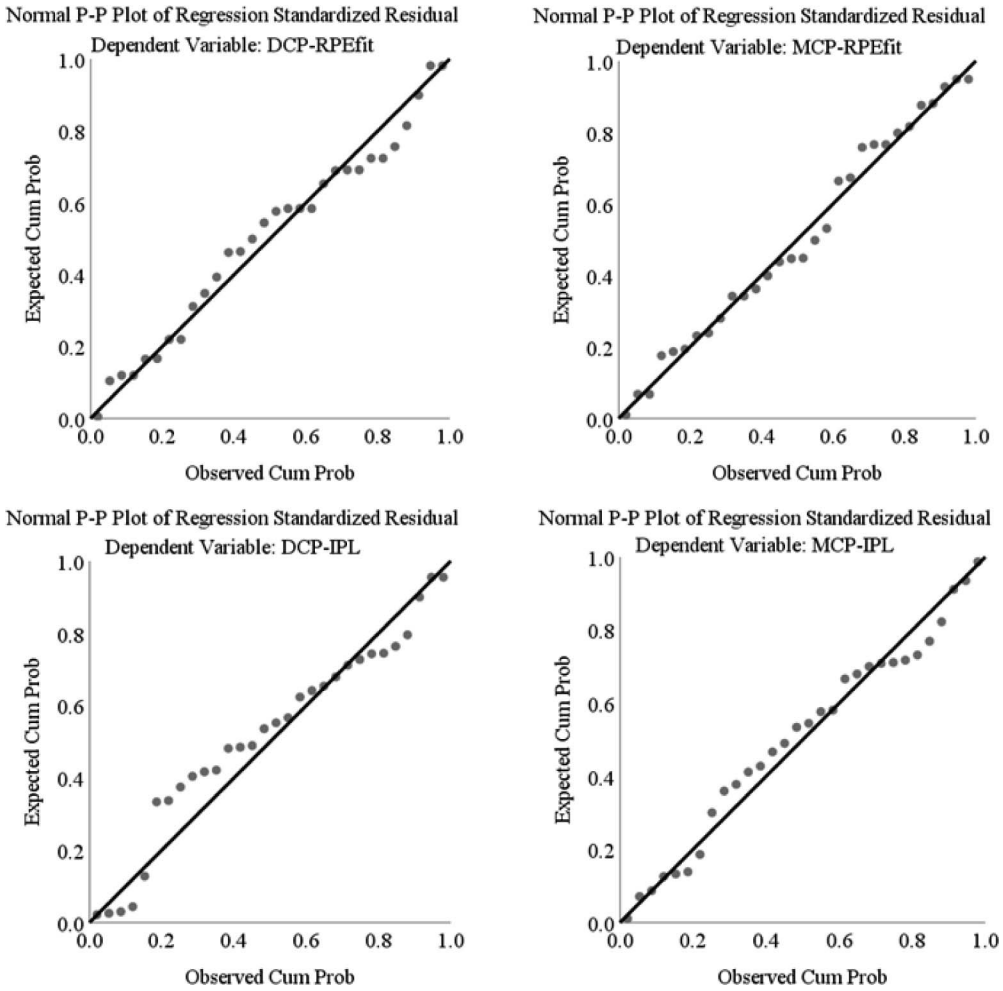

Figure 5. Normal P-P plot of regression standardized residual. (A) The estimated DCP position with RPEfit as the reference line is the dependent variable. (B) The estimated MCP position with RPEfit as the reference line is the dependent variable. (C) The estimated DCP position with IPL as the reference line is the dependent variable. (D) The estimated MCP position with IPL as the reference line is the dependent variable. (B) Shows a better prediction accuracy, follow by (A) and (D).

mental studies, at 25 to 26 weeks of gestation, deeper plexus components form by angiogenic sprouting from the primary plexus veins, and these plexus sprouts penetrate the retina and establish two laminar networks on either side of the INL.[10,22,26–28] Additionally, Tan and his colleagues[8] found four layers of capillary plexuses in the human retina through anatomical studies of cadaveric eyes, which are located on the nerve fiber layer, retinal ganglion cell, border of the IPL and superficial boundary of the INL, and boundary of the deep INL and OPL. These findings are in perfect agreement with our study.

In our study, the estimated position of MCP was affected by CRT and GCT regardless of whether we used RPEfit or IPL as the reference line. According to linear regression analysis, to achieve the best fitting

Table 4. VD and SD of the Three Capillary Plexuses[a]

	SCP	MCP	MCP-re	DCP	DCP-re
VD (%)	32.97 ± 3.90	45.05 ± 5.34	57.52 ± 7.11	37.34 ± 4.96	33.42 ± 4.80
SD (mm^{-1})	14.45 ± 1.51	19.80 ± 1.92	23.52 ± 2.10	17.38 ± 1.97	15.61 ± 1.93

[a] Data are the mean ± standard deviation, MCP-re means the MCP after removal of the decorrelation tail artifact, and DCP-re means the DCP after removal of the decorrelation tail artifact.

Table 5. ICCs and RSDs Analyzed for VD and SD[a]

	SCP	MCP	MCP-re	DCP	DCP-re
ICC					
VD	0.996	0.971	0.984	0.950	0.941
SD	0.996	0.963	0.971	0.948	0.931
RSD					
VD (%)	-	1.36	1.49	1.27	2.26
SD (%)	-	1.34	0.61	1.22	1.46

[a] MCP-re means the MCP after removal of the decorrelation tail artifact, and DCP-re means the DCP after removal of the decorrelation tail artifact.

degree, we used RPEfit as the reference line to locate MCP and the outer boundary of MCP = 14.491 − 0.307 CRT − 1.443 GCT. For every micrometer increase in CRT, the estimated MCP position increased by 0.307 microns, while for every micrometer increase in GCT, the estimated MCP position increased by 1.443 microns. Although the unstandardized coefficient of CRT is smaller than that of GCT, CRT has a greater effect on MCP estimated location than GCT (standardized coefficient 0.493 vs. 0.362). The position of the DCP relative to RPEfit was affected by GCT, and the position relative to IPL was not affected by either area. Therefore, using IPL as the reference line for the estimated position of DCP is appropriate, and the outer boundary of DCP is 37.63 ± 7.04 μm below IPL. Consequently, placing the MCP in a position relative to the IPL as performed in previous studies might be inappropriate.[15–17]

Here, the MCP had the highest VD, followed by the DCP and SCP. Based on our results and other studies of human histology, the MCP lies at the boundary of the IPL and inner portion of the INL, colocalizing with the bipolar cell processes and amacrine cells in close proximity to the high oxygen demand of the IPL synapses,[11] whereas the DCP lies at the boundary of the deep INL and OPL, colocalizing with horizontal cells and close to the OPL synapses.[29] Retinal oxygen measurement experiments in animal models have determined that the primary oxygen consumers of the inner retinal layer are located in the plexiform layers (IPL and OPL), which may be located in mitochondria-rich synapses.[30,31] Areas with high oxygen consumption tend to have thinner blood vessels and higher blood flow density to provide a higher surface area-to-blood volume ratio for material exchange.[32,33] In a report by Onishi et al.,[15] the VD of the SCP was 48.19% ± 2.95%, and the VDs of the MCP and DCP without decorrelation tail artifact removal were 56.71% ± 2.73% and 59.87% ± 3.32%, respectively. In the RTVue XR Avanti OCTA system, the calculation area of VD was in the parafoveal region, which was defined as a ring around the fovea with an inner ring diameter of 1 mm and an outer ring diameter of 3 mm. Therefore, the partial or whole FAZ was excluded from the total area, and the results were relatively high.[15,34–36]

In the study by Garrity et al.,[17] the SD values of the SCP, MCP, and DCP were 15.48 ± 2.04 mm^{-1}, 15.28 ± 1.82 mm^{-1}, and 16.33 ± 2.32 mm^{-1}, respectively, while projection artifacts were removed from en face OCTA images of the MCP and DCP with three-dimensional PAR-enabled software developed by Optovue.[37,38] In our study, the values of the SCP and DCP after removal of decorrelation tail artifacts were very close to the results of Garrity et al. (14.45 ± 1.51 mm^{-1} vs. 15.48 ± 2.04 mm^{-1} and 15.61 ±1.93 mm^{-1} vs. 16.33 ± 2.32 mm^{-1}), but the results of the MCP were very different (23.52 ± 2.10 mm^{-1} vs. 15.28 ± 1.82 mm^{-1}). As shown in Figure 4, the commercial software on the AngioPlex platform can remove the artifacts in the DCP well, whereas in the MCP, it reduces only the grey value of the decorrelation tail artifacts of the upper layer. Because the artifact was not completely removed, the artifact was still considered an OCTA blood flow signal when performing the VD calculation. The method reduces the artifacts by comparing and reconstructing two slab images generated from two or more retinal layers.[20,39] When the signal of the upper layer is too strong or signals affect adjacent multiple layers, the artifact cannot be completely eliminated. Interestingly, this approach can improve the signal-to-noise ratio of the FAZ in the MCP, resulting in a lower threshold value and even a higher VD (Table 4). The projection-resolution algorithm of the AngioVue platform is compared along each axial scan in the proximal to distal direction, identifying successive higher peaks as real vessels and removing smaller peaks.[40,41]

The present study has limitations. First, we report the values for only a small population of healthy subjects. Further studies are needed to establish a normative database of retinal segmentation. Second, the analysis of diseased eyes is beyond this report. In some diseases, such as diabetes, hypertension, glaucoma, high myopia, and age-related macular degeneration, the structure of the retina and vessels may change, leading to different segmentation results. Moreover, as mentioned above, the artifact in the

MCP cannot be completely removed, so the value of the VD and SD in the MCP may be affected. We expect the emergence of a more advanced method of artifact removal by the instrument. Finally, although we determined the general position of the three layers of capillary plexuses in the retina, our results could not be directly applied to other platforms due to the different definitions of the reference line by different OCT platforms.

In conclusion, by using the progressive matching method, we segmented three capillary plexuses visually and defined the relative positions of each capillary plexus to the reference line, which provided convenience for future studies. Moreover, we calculated the VD and SD of three capillary plexuses in some normal subjects, providing controls for future studies.

Acknowledgments

Supported by Suzhou Science and Technology Bureau (no. SS201758) (no. SYS2018004), Jiangsu Distinguished Medical Experts Program (no. 2016), Gusu Health Leading Talent Plan (grant no. 025), and Technology Program of Soochow City (no. SYS201375).

Disclosure: **Q. Zhu**, None; **X. Xing**, None; **M. Zhu**, None; **H. Xiao**, None; **L. Ma**, None; **L. Chen**, None; **J. Liang**, None; **Y. Yuan**, None; **E. Song**, None

References

1. Kim AY, Chu Z, Shahidzadeh A, et al. Quantifying microvascular density and morphology in diabetic retinopathy using spectral-domain optical coherence tomography angiography. *Invest Ophthalmol Vis Sci*. 2016;57:OCT362–OCT370.
2. Kim AY, Rodger DC, Shahidzadeh A, et al. Quantifying retinal microvascular changes in uveitis using spectral-domain optical coherence tomography angiography. *Am J Ophthalmol*. 2016;171:101–112.
3. Kashani AH, Chen CL, Gahm JK, et al. Optical coherence tomography angiography: a comprehensive review of current methods and clinical applications. *Prog Retin Eye Res*. 2017;60:66–100.
4. Lei J, Yi E, Suo Y, et al. Distinctive analysis of macular superficial capillaries and large vessels using optical coherence tomographic angiography in healthy and diabetic eyes. *Invest Ophthalmol Vis Sci*. 2018;59:1937–1943.
5. Durbin MK, An L, Shemonski ND, et al. Quantification of retinal microvascular density in optical coherence tomographic angiography images in diabetic retinopathy. *JAMA Ophthalmol*. 2017;135:370.
6. Tan ACS, Tan GS, Denniston AK, et al. An overview of the clinical applications of optical coherence tomography angiography. *Eye (Lond)*. 2017;32(2):262–286.
7. Li M, Yang Y, Jiang H, et al. Retinal microvascular network and microcirculation assessments in high myopia. *Am J Ophthalmol*. 2017;174:56–67.
8. Tan PE, Yu PK, Balaratnasingam C, et al. Quantitative confocal imaging of the retinal microvasculature in the human retina. *Invest Ophthalmol Vis Sci*. 2012;53:5728–5736.
9. Lutty GA, McLeod DS. Development of the hyaloid, choroidal and retinal vasculatures in the fetal human eye. *Prog Retin Eye Res*. 2018;62:58–76.
10. Selvam S, Kumar T, Fruttiger M. Retinal vasculature development in health and disease. *Prog Retin Eye Res*. 2018;63:1–19.
11. Usui Y, Westenskow PD, Kurihara T, et al. Neurovascular crosstalk between interneurons and capillaries is required for vision. *J Clin Invest*. 2015;125:2335–2346.
12. Kornfield TE, Newman EA. Regulation of blood flow in the retinal trilaminar vascular network. *J Neurosci*. 2014;34:11504–11513.
13. Biesecker KR, Srienc AI, Shimoda AM, et al. Glial cell calcium signaling mediates capillary regulation of blood flow in the retina. *J Neurosci*. 2016;36:9435–9445.
14. Hagag AM, Pechauer AD, Liu L, et al. OCT angiography changes in the 3 parafoveal retinal plexuses in response to hyperoxia. *Ophthalmol Retina*. 2018;2:329–336.
15. Onishi AC, Nesper PL, Roberts PK, et al. Importance of considering the middle capillary plexus on OCT angiography in diabetic retinopathy. *Invest Ophthalmol Vis Sci*. 2018;59:2167–2176.
16. Park JJ, Soetikno BT, Fawzi AA. Characterization of the middle capillary plexus using optical coherence tomography angiography in healthy and diabetic eyes. *Retina*. 2016;36:2039–2050.
17. Garrity ST, Iafe NA, Phasukkijwatana N, et al. Quantitative analysis of three distinct retinal capillary plexuses in healthy eyes using optical

coherence tomography angiography. *Invest Ophthalmol Vis Sci*. 2017;58:5548–5555.
18. Nesper PL, Fawzi AA. Human Parafoveal capillary vascular anatomy and connectivity revealed by optical coherence tomography angiography. *Invest Ophthalmol Vis Sci*. 2018;59: 3858–3867.
19. Gao SS, Jia Y, Zhang M, et al. Optical coherence tomography angiography. *Invest Ophthalmol Vis Sci*. 2016;57:OCT27–OCT36.
20. Bagherinia H, Knighton RW, De Sisternes L, et al. A fast method to reduce decorrelation tail artifacts in OCT angiography. *Invest Ophthalmol Vis Sci*. 2017;58:643–643.
21. Rasband WS. ImageJ. U.S. National Institutes of Health, Bethesda, Maryland. Available at: http://imagej.nih.gov/ij/, 1997–2016. Accessed December 10, 2017.
22. Provis JM. Development of the primate retinal vasculature. *Prog Retin Eye Res* 2001;20:799–821.
23. Salas M, Augustin M, Ginner L, et al. Visualization of micro-capillaries using optical coherence tomography angiography with and without adaptive optics. *Biomed Opt Express*. 2017;8:207–222.
24. Fouquet S, Vacca O, Sennlaub F, et al. The 3D retinal capillary circulation in pigs reveals a predominant serial organization. *Invest Ophthalmol Vis Sci*. 2017;58:5754–5763.
25. Bonnin S, Mane V, Couturier A, et al. New insight into the macular deep vascular plexus imaged by optical coherence tomography angiography. *Retina*. 2015;35:2347–2352.
26. Fruttiger M. Development of the retinal vasculature. *Angiogenesis*. 2007;10:77–88.
27. Hughes S, Yang H, Chan-Ling T. Vascularization of the human fetal retina: roles of vasculogenesis and angiogenesis. *Invest Ophthalmol Vis Sci*. 2000;41:1217–1228.
28. Gariano RF, Iruela-Arispe ML, Hendrickson AE. Vascular development in primate retina: comparison of laminar plexus formation in monkey and human. *Invest Ophthalmol Vis Sci*. 1994;35:3442–3455.
29. Chan G, Balaratnasingam C, Yu PK, et al. Quantitative morphometry of perifoveal capillary networks in the human retina. *Invest Ophthalmol Vis Sci*. 2012;53:5502–5514.
30. Yu DY, Cringle SJ, Su EN. Intraretinal oxygen distribution in the monkey retina and the response to systemic hyperoxia. *Invest Ophthalmol Vis Sci*. 2005;46:4728–4733.
31. Yu DY, Cringle SJ, Yu PK, et al. Intraretinal oxygen distribution and consumption during retinal artery occlusion and graded hyperoxic ventilation in the rat. *Invest Ophthalmol Vis Sci*. 2007;48:2290–2296.
32. Bell MA, Ball MJ. Morphometric comparison of hippocampal microvasculature in ageing and demented people: diameters and densities. *Acta Neuropathol*. 1981;53:299–318.
33. Pawlik G, Rackl A, Bing RJ. Quantitative capillary topography and blood flow in the cerebral cortex of cats: an in vivo microscopic study. *Brain Res*. 1981;208:35–58.
34. Dimitrova G, Chihara E, Takahashi H, et al. Quantitative retinal optical coherence tomography angiography in patients with diabetes without diabetic retinopathy. *Invest Ophthalmol Vis Sci*. 2017;58:190–196.
35. Al-Sheikh M, Phasukkijwatana N, Dolz-Marco R, et al. Quantitative OCT angiography of the retinal microvasculature and the choriocapillaris in myopic eyes. *Invest Ophthalmol Vis Sci*. 2017; 58:2063–2069.
36. Zahid S, Dolz-Marco R, Freund KB, et al. Fractal dimensional analysis of optical coherence tomography angiography in eyes with diabetic retinopathy. *Invest Ophthalmol Vis Sci*. 2016;57: 4940–4947.
37. Maruko I, Spaide RF, Koizumi H, et al. Choroidal blood flow visualization in high myopia using a projection artifact method in optical coherence tomography angiography. *Retina*. 2017;37:460–465.
38. Chetrit M, Bonnin S, Mane V, et al. Acute pseudophakic cystoid macular edema imaged by optical coherence tomography angiography. *Retina*. 2018;38:2073–2080.
39. Bagherinia H. A novel approach to reducing decorrelation tail artifacts in optical coherence tomography angiography. Seattle, WA: Association for Research in Vision and Ophthalmology; 2016.
40. Zhang M, Hwang TS, Campbell JP, et al. Projection-resolved optical coherence tomographic angiography. *Biomed Opt Express*. 2016; 7:816–828.
41. Hwang TS, Zhang M, Bhavsar K, et al. Visualization of 3 distinct retinal plexuses by projection-resolved optical coherence tomography angiography in diabetic retinopathy. *JAMA Ophthalmol*. 2016;134:1411–1419.